RSC Advances

ROYAL SOCIETY OF CHEMISTRY

www.rsc.org/advances

Journal Name

ARTICLE

Synthesis and properties of a millable polyurethane nanocomposite based on castor oil and halloysite nanotube

Received 00th January 20xx,
Accepted 00th January 20xx

DOI: 10.1039/x0xx00000x

www.rsc.org/

Bing Gong,[a] Chunfa Ouyang,*[a] Qun Gao,[a] Liang Zhao[a] and Zhengchuang Zhao[a]

The use of bio-based materials is recently attracting high attention in the polymer synthesis. In this work, a bio-based millable polyurethane (MPU) based on castor oil and its nanocomposites contained very low content of halloysite nanotubes have been successfully prepared. This MPU/HNTs nanocomposites showedhigher tensile strength and elongation at break comparing with pristine MPU material. The tensile strength and Young's modulus of MPU/HNTs nanocomposites wereimproved 35% and 63% by incorporating only 0.5 wt% of HNTs, respectively,which was primarily attributed to the formation of covalent bonds between the OH groups of HNTs and the NCO groups of 2,4-toluene diisocyanate (TDI). The nanostructure of these MPU nanocomposites were characterized by spectroscopy studies and direct microstructural analysis.

Introduction

Polymer nanocomposites reinforced with low fraction of nanoscale fillers containing organic and inorganic have drawn a great deal of attention owing to the unique characteristics of nanoparticles, includingtheir large surface area, high surface reactivity, and relative low cost.[1-3] Nowadays, with the strengthening of environmental legislation and awareness of environmental protection, the use of vegetable oil is worth being highly taken into consideration since it offers the intrinsic value of reduced toxicity, low cost, high purity and its availability as a renewable agricultural resource.[4-6] Castor oil (CO) is a commercially available naturally occurring vegetable oil owing free secondary hydroxyl groups (Scheme 1), which including about 90% of the fatty acid is ricinoleic acid and the others are mainly oleic and linoleic acids. Ricinoleic acid is an 18-carbon acid with a double bond between the 9 and 10 carbon atom positions and a hydroxyl group on the 12th carbon atom.[7,8] This combination of hydroxyl group and unsaturation occurs only in CO, CO is suitable in isocyanate's reactions to make polyurethane elastomers owing to its hydroxyl functionality.

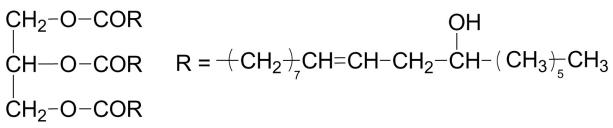

Scheme 1 Structure of castor oil.

Halloysite nanotubes (HNTs), $Al_2Si_2O_5(OH)_4 \cdot nH_2O$, one of naturally occurring clay minerals, is a new kind of prominent nanofillers composed of multi-walled nanotubular-shaped crystalline nanostructures.[9] Generally, HNTs have a 15-20 nm lumen with 30-50 nm external diameter and length of around 100-1500 nm. HNTs consist of gibbsite octahedral sheet (Al-OH) groups on the internal surface and siloxane groups (Si-O-Si) on the external surface, which have been successfully applied in the sustained drug and flame retardant release.[10,11] HNTs have been incorporated into polymer matrix as an environmentally benign reinforcing fillers due to their outstanding intrinsic properties such as nanoscale dimensions, high surface area, unique morphology, low density, high specific strength and Young's modulus, and very low coefficient of thermal expansion.[12-16] Polyurethane (PU) elastomers can be divided into three different types depending upon their structure, i.e., castable polyurethane (CPU), thermoplastic polyurethane (TPU), and millable polyurethane (MPU). MPUare a special type of synthetic rubber, which are generally compounded by means of conventional rubber processing equipments in the presence of other ingredients/additives.[17-20] MPUstillhave an excellent demand in various applications such as footwear, hose and oil field products owing to its high toughness, flexibility, strength, abrasion resistance, and chemical resistance. Many large industrial rolls, copier rolls, O-rings,seals, gaskets and many other mechanical goods requiring abrasion resistance are made using these special elastomers.[21-30] The basic constituents of PU elastomers are a diisocyanate, a long chain oligomeric polyol, which may be a polyether or polyester oligomer,and low molecular weight diols or diamines as chain extender.[31] Previously, nanometer-sized materials including graphite oxide nanoplatelets,[32] polyhedral oligomeric silsesquioxane,[33,34]carbon nanotubes,[35-38]and layered silicate clays,[39-43]which own an extremely large

[a] School of Materials Science and Engineering,Shanghai Institute of Technology, 100 Haiquan Road, Shanghai 201418, China.
Electronic Supplementary Information (ESI) available: See DOI: 10.1039/x0xx00000x

surface area or a high aspect ratio have been incorporated into CPU or TPU to enhance the mechanical performances and thermal stability.

Although there are many reports in the literature concerning PU nanocomposites, no comprehensive notice has so far been given to the MPU nanocomposites. In the few relevant literature, nanomaterials have been added into MPU which has been purchased in advance only in the later process by mechanical mixing to prepare its nanocomposites.In the present study, we introduce HNTs which not only have special surface properties, but also havethe advantages of wide source and low cost into the synthesis of MPU for the first time to stiffen and strengthen the material at very low loadings. In addition, we report the preparation ofMPU using HNTs, modifiedCOblended with polytetramethylene ether glycol (PTMEG 650) with different molar ratios of 1,4-butane diol (BD) as chain extender and 2,4-toluene diisocyanate (TDI).

Experimental section

Materials

Because the preparations involved toxic and reactive isocyanates, all the necessary precautions for their safe handling and for conducting their reactions under anhydrous conditions were taken in all the experimental work.

2,4-tolylene diisocyanate (TDI, YMIOO chemical), 1,4-butanediol (BD, Aldrich), diethyleneglycolmonoethylether (Aldrich) and polytetramethylene ether glycol (PTMEG 650, SIGMA- ALDRICH) were used as received.Castor oil (CO) having the hydroxy number (#OH) 159 mgKOH/g was supplied from Sinopharm Chemical Reagent Co., Ltd. (China). Halloysite nanotubes (HNTs), with 15-20 nm lumens and 30-50 nm external diameter and approximate length of 100-1500 nm were purchased from Lingshou Longchuan drilling plugging materials factory (China) without any chemical modification.

Synthesis of terminated TDI

In a four-necked, round-bottomed flask equippedwith a stirrer, dropping funnel, thermometer and oilbath was placed for TDI (220 g). The temperature was brought to 50 °C, followed by dropwise addition of diethyleneglycolmonoethylether (169.6 g) under stirring. The droping process was continued around for 3 h and then the process of detecting isocyanate content was conducted. The reaction was ended until the isocyanate content reached about 12.75 %. The terminated TDI was obtained by the reaction between diethyleneglycolmonoethylether and TDI (Scheme 2).

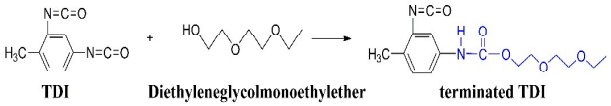

Scheme 2 Reaction scheme for the synthesis of terminated TDI.

For Fig. 2: ^{1}H NMR (600 MHz, DMSO) : δ (ppm) = 9.81 (s, 7H,–NH–), 8.86 (d, 3H), 8.07-7.92 (m, 4H), 7.48 (dd, 4H), 7.43-7.29 (m, 9H, =CH–C–), 7.29-6.84 (m, 40H, =CH–CH=), 6.84-6.68 (m, 4H), 4.83-4.66 (m, 4H), 4.36-4.02 (m, 52H, –O–CH_2–), 3.68-3.59 (m, 40H, –CH_2–O–), 3.59-3.46 (m, 98H, –CH_2–CH_2–), 3.46-3.38 (m, 50H,–O–CH_2–), 2.23 (d, 60H, –CH_3), 1.08-0.96 (m, 78H,–CH_3).

^{13}C NMR (151 MHz, DMSO) : δ (ppm) =154.68 (s), 154.53 (s), 154.32-153.67 (m), 138.75 (s), 138.03 (dd), 137.80 (d), 136.76 (d), 132.25 (s), 132.09 (s), 131.37 (d), 130.84 (d), 130.39 (d), 126.48 (s), 126.17 (d), 124.70 (d), 116.22 (s), 115.36 (s), 114.60 (s), 70.33 (d), 69.72 (s), 69.41-69.02 (m), 66.96 (s), 66.06 (d), 64.23 (s), 64.26-63.40 (m), 40.16 (s), 40.02 (s), 39.88 (s), 39.85-39.42 (m), 39.46 (s), 39.39 (d), 18.20-17.59 (m), 17.41 (d), 15.33 (s).

Synthesis of difunctional CO

In a four-necked, round-bottomed flask equipped with a stirrer, dropping funnel, thermometer and oil bath was placed dried CO (200 g). The temperature was brought to 100 °C, followed by dropwise addition of the synthetic terminated TDI (110.88 g) under stirring. The reaction was continued for 2 h and then cooled and kept well stoppered. The difunctional CO was obtained by following procedure (Scheme 3).

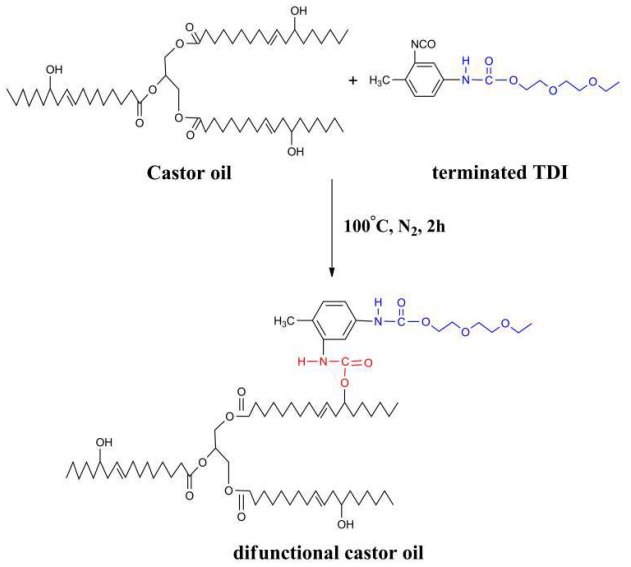

Scheme 3 Reaction scheme for the synthesis of difunctional CO.

For Fig. 4: ^{1}H NMR (600 MHz, DMSO) : δ (ppm) = 7.50 (d, J = 30.3 Hz, 7H), 7.20-7.08 (m, 8H), 7.05 (t, J = 8.8 Hz, 9H), 5.44 (s, 8H), 5.41-5.12 (m, 31H), 4.84-4.59 (m, 8H), 4.40-4.31 (m, 7H), 4.31-4.20 (m, 11H), 4.20-4.01 (m, 29H), 3.63 (d, J = 3.2 Hz, 18H), 3.59-3.21 (m, 221H), 2.50 (dt, J = 3.6, 1.8 Hz, 323H), 2.28 (s, 12H), 2.28-2.23 (m, 35H), 2.28-2.20 (m, 38H), 2.28-1.73 (m, 118H), 2.28-1.93 (m, 116H), 2.28-1.72 (m, 118H), 2.28-1.53 (m, 123H), 2.28-0.65 (m, 545H), 0.85 (dd, J = 6.9, 5.2 Hz, 51H), 0.85 (dd, J = 6.9, 5.2 Hz, 54H), 0.11-0.05 (m, 20H).

^{13}C NMR (151 MHz, DMSO) : δ (ppm) = 172.50 (d, J = 44.7 Hz), 172.34-171.84 (m), 154.57 (s), 153.80 (s), 137.69 (s), 136.94 (d, J = 16.3 Hz), 132.33 (s), 130.54 (d, J = 38.2 Hz), 129.99 (s), 128.07 (s), 127.06 (s), 126.28-124.42 (m), 115.34 (s), 73.82 (s), 70.32 (s), 69.76 (d, J = 7.1 Hz), 69.64- 68.96 (m), 66.10 (d, J = 4.1 Hz), 63.89 (d, J = 24.9 Hz), 62.20 (s), 40.35 (s),

40.14 (d, J = 20.9 Hz), 39.93 (s), 39.79 (s), 39.72-38.99 (m), 37.04 (s), 35.68 (s), 34.12-33.58 (m), 32.29 (d, J = 20.2 Hz), 32.02 (s), 31.89 (dd, J = 26.5, 8.4 Hz), 29.53 (dd, J = 34.3, 24.8 Hz), 29.07 (d, J = 32.2 Hz), 28.96-28.62 (m), 27.35 (s), 27.15 (s), 25.96-25.58 (m), 25.39 (s), 24.89 (s), 22.81-22.37 (m), 17.53 (d, J = 8.6 Hz), 15.45 (d, J = 6.7 Hz), 14.26 (s).

Synthesis of millable polyurethane elastomers nanocomposites

The required amounts of polyols, chain extender and nanofiller were added to the resin kettle in which N_2 atmosphere was maintained. The mixture was stirred vigorously for 10-60 mins, and then TDI was added in a lot and the mixture continually stirred for 3-10 mins. Then it was casted into preheated aluminum trays coated with Teflon, heated in an oven at 75 °C for 8 h. The formulations designed for the synthesis of the nanocomposites were given in Table 1. The concentration of reactive hydroxyl groups on HNTs was 29 ± 3 mmol/g, and was measured using titration to determine the excessive isocyanate groups after mixing HNTs with a known amount of TDI. The total NCO/OH ratio in the polyurethane was 0.95. Transparent polyurethane nanocomposite films containing 0.5, 1, and 5 wt % HNTs were successfully prepared by varying the amount of HNTs and 1,4-BD, and coded as D-0.5, D-1, D-5, respectively. Pure polyurethane films were prepared in the absence of HNTs and coded as D. The reaction procedure is illustrated as follows in Scheme 4. It should be noted that what is expressed as the hard segment in Scheme 4 was composed of TDI and 1,4-BD, whereas that denoted as the soft segment was composed of difunctional CO and PTMEG.

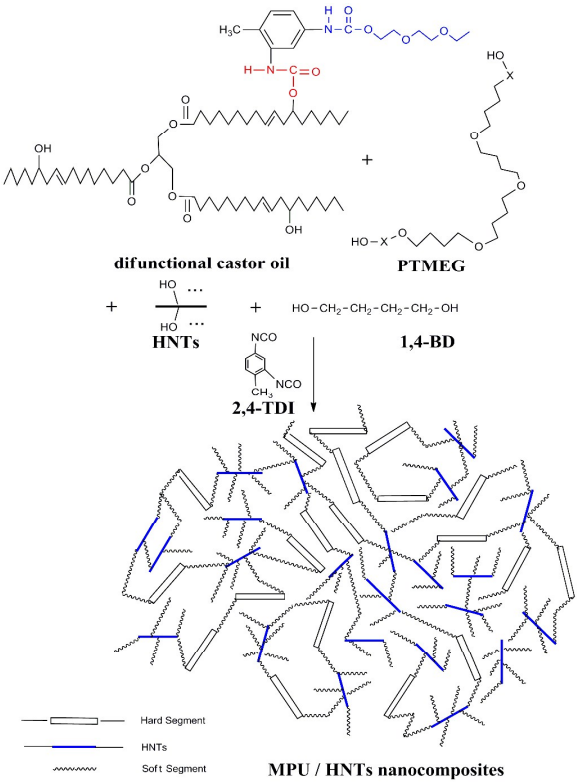

Scheme 4 Reaction scheme for the synthesis of elastomeric gum polyurethanes nanocomposites.

Table 1 Compositions of elastomeric gum polyurethanes nanocomposites

sample	Weight of CO /(g)	Weight of PTMEG (650) /(g)	Weight of HNTs /(g)	Weight of BD /(g)	Weight of TDI /(g)	NCO / OH ratio
D	119.88	84.24	0	60.12	152.82	0.95
D-0.5	119.88	84.24	2.07	57.33	152.82	0.95
D-1	119.88	84.24	4.14	54.63	152.82	0.95
D-5	119.88	84.24	20.7	33.03	152.82	0.95

Characterizations

Fourier transform infrared (FTIR) spectra were obtained on an iZ™ 10 spectrometer (Nicolet, USA), and each spectrum was comprised of 16 scans with a resolution of 4 cm^{-1}. Proton nuclear magnetic resonance (^1H and ^{13}C NMR) spectra were recorded on an AVANCE III NMR spectrometer (Bruker Corp). Dimethyl sulphoxide (DMSO-d6) was used as the solvent, respectively and the measurements were conducted at 400 MHz. The chemical shifts in the discussion are reported in ppm. The SERS measurement was conducted on the Renishaw in Via-Reflex micro-Raman spectrometer equipped with 532 nm laser. The Raman spectrum was calibrated using silicon substrate (532 nm calibration peak). The sample was exposed by the laser for 2 s every time and was scanned for 5 times under 1 % total laser power.

Chromatographic separations were performed on an ACQUITY™ UPLC System (Waters Corporation, Milford, MA), The separation of the sample was performed on a Waters Acquity BEH C_{18} column (2.1 mm×100 mm, 1.7 μm) (Waters Corporation, Milford, USA). The column was maintained at 30 ℃ with a flow rate of 0.4 mL/min. The mobile phase was composed of water (Phase A) and acetonitrile (Phase B) and the optimized gradient elution program was set as follows: 0-3 min: 1-10 % B; 3-6 min: 10-40 % B; 6-8.5 min: 40-100 % B; 8.5-10.2 min: 100 % B; 10.2-10.8 min: 100-99 % B; 10.8-12.6 min: 1 % B.

MS spectrometry was carried out on a Waters Q-TOF Premier MS system (Waters Corp., Milford, MA) with an electrospray ionization source (ESI) operating in positive ion mode. Nitrogen was used as the drying gas .The desolvation gas flow rate was 700 L/h at 350 ℃. Cone gas flow rate was maintained at 50 L/h and the source temperature was set at 120 ℃. Capillary voltage and cone voltage were 3.0 kV and 40 V respectively. The scan time and interscan delay were 0.28 s and 0.1 s, respectively.

X-ray diffraction (XRD) measurements were conducted on a D/max 2200 PC X-ray diffractometer (Rigaku Corp., Japan) equipped with a CuK radiation source (50.1540 nm, operated at 40 kV and 30 mA) over a 2θ range of 5° to 40° with a scan speed of 2°/min. Thermogravimetric analysis (TGA) was conducted with an STA 499 F3 Jupiter® (NETZSCH, Germany) with N_2 as the purge gas at a flow rate of 40 ml/min. Samples (8 – 12 mg) were heated from room temperature to 700 ℃ at a heating rate of 10 ℃/min. Atomic force microscopy (AFM) images were obtained by an AFM instrument (Beijing Nano-Instruments, Ltd., China) operating in the tapping mode using silicon cantilevers (spring constant: 3 – 40 Nm^{-1}; cantilever resonant frequency: 75 – 300 KHz).

Dynamic mechanical analysis (DMA) was conducted on a DMA 242 C dynamic mechanical analyzer (NETZSCH, Germany) over a temperature range of −100 ℃ to 170 ℃ at a heating rate of 3 ℃/min and a frequency of 1 Hz. Transmission electron microscopy (TEM) was conducted using a JEM-2010 high resolution field emission microscope (Jeol, Ltd., Japan) operating at 200 kV, providing a lattice resolution of 0.14 nm. The mechanical properties of the products were measured following the GB/T 528-1998 standard using a SUN 500 universal testing machine (GALDABINI, Italy). The crosshead speed was 50 mm/min. All measurements were repeated five times, and the averages were obtained. The hardness of the products were measured by a Shore A hardness tester following the ASTM D 2240-2004 standard. All hardness measurements in this report were conducted after 10 s when the indenter had penetrated into the composites.

Results and discussion

Since difunctional polyols were needed in the preparation of MPU, the trifunctional part of CO had to be changed to difunctional moieties. This had been achieved by reacting the appropriate amount of the synthetic terminated TDI with a certain amount of CO. Eq. (1) showed the relation between functionality (f), molecular weight (MW) and hydroxy number:[8]

$$\frac{MW}{f} = \frac{56100}{\#OH} \quad (1)$$

According to the measured data for unmodified CO (#OH=185 mg KOH/g and MW=932 g/mol) the average functionality of CO would be f=3.07. In the same manner f=2 corresponded to #OH =120 mg KOH/g. So the reduced amount of #OH should be 185-120=65 mg KOH/g, which was equal to 0.0012 mole KOH and this was corresponding to the mole of the synthetic terminated TDI (MW=308 g/mol) needed for the preparation of 1 g CO with average functionality of 2.

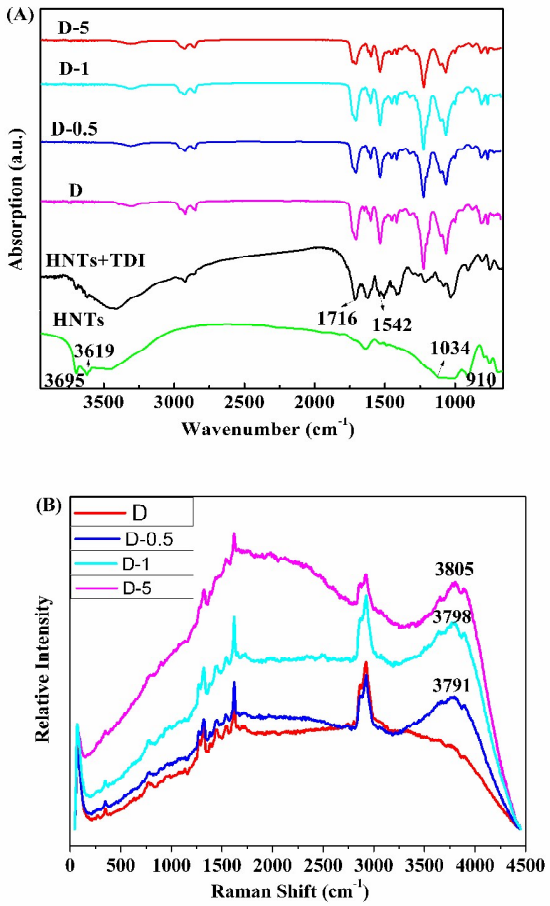

Fig. 1 (A) FTIR spectra of HNTs, MPU/HNTs nanocomposites, and a control mixture of HNTs and TDI. (B) Raman spectra of MPU/HNTs nanocomposites.

The FTIR spectra of HNTs, pristine MPU, various MPU/HNTs nanocomposites, and a control sample comprised of a mixture of HNTs and TDI, are shown in Fig 1(A). To help investigate the interfacial interaction between HNTs and the MPU matrix, a control sample comprised of a mixture of HNTs and TDI was prepared by reacting TDI (10 g) with HNTs (3.96 g), and dispersing in DMAC (20 g) at 82 ℃ for 3 h. Subsequently, the solvent was evaporated at 100 ℃ for 6 h in a vacuum oven. FTIR spectra of the pure MPU showed characteristic bands of urethane stretching (N–H) at 3304 cm^{-1}, combination of urethane carbonyl (NH-CO-O) and esteric carbonyl (CO-O) at 1716 cm^{-1}, combination of N–H out-of-plane bending and C–N stretching at 1550-1520 cm^{-1}. The asymmetric stretching vibration absorption peak of a saturated methylene -CH_2- was detected near at 2860 cm^{-1}. The asymmetric vibration absorption peaks and the symmetric vibration absorption peak of -C-O-C- were detected at 1220 cm^{-1} and 1110 cm^{-1}, respectively. In the HNTs, O-H of inner hydroxyl groups and outer surface hydroxyl groups were detected at 3619 cm^{-1} and 3695 cm^{-1}, respectively. The infrared spectrum showed absorption bands around 1034 cm^{-1} and 910 cm^{-1}, which were

attributed to the Si-O stretching vibrations and Al-OH vibrations bands, respectively.[13]

For all the spectra of nanocomposites, the intensity of the absorption near 3695 cm^{-1} and 3619 cm^{-1} greatly decreased, which were due to the reaction of the OH group of HNTs with the NCO group of TDI. Similarly, the band of NCO group was not detected at 2300-2200 cm^{-1} in the products as a result of complete reaction, which confirmed the reaction of the OH group of HNTs with the NCO group of TDI and thus further implied that the OH group of HNTs was covalently bonded to the polyutethane molecular chains. Analogously, a combination of NH-CO-O andCO-Owas detected at 1716 cm^{-1}, and N-H out-of-plane bending was detected at 1542 cm^{-1} in the control sample as a result of the generation of urethane bonds, which confirmed the reaction between NCO groups of TDI and OH groups of HNTs, as illustrated in Scheme 5.

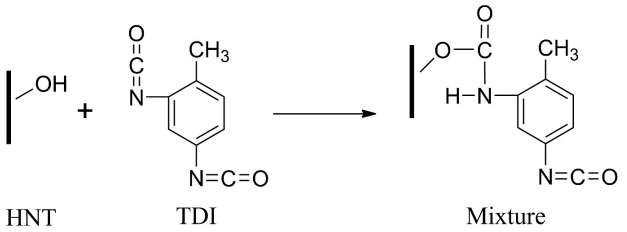

Scheme 5 Reaction scheme between a single OH of an HNT and TDI.

Fig. 1(B) showed Raman spectra of MPU/HNTs nanocomposites. The neat MPU exhibited peaks at 861, 968, 1182, 1246 and 1310, 1614, and 2932 cm^{-1} indicating C-O-C bending, C-H aromatic ring bending, C-O-C symmetrical stretching, C-N stretching, C=C stretching, and C-H stretching, respectively. Similar peaks were observed for nanocomposites compared to neat MPU. The characteristic bands of inter hydroxy-vibration of lower plane in the halloysite octahedral sharing layers were investigated at 3619 cm^{-1} in HNTs. The interaction of hydrogen bonding and dioctahedral space formed three different condition of inter hydroxy, which because of the hydroxy inserted within the adjacent space. The absorption peak at 3695 cm^{-1} was observed corresponding to outer hydroxy-vibration of the outside unshared octahedral plane, which might due to the dislocation of folding octahedral layer.[43] Obviously, the characteristic absorption peaks of HNTs around at 3600-3700 cm^{-1} were observed and the peak position shifted to higher with increasing HNTs content in the nanocomposites, which further confirmed the reaction of the OH group of HNTs with the NCO group of TDI.

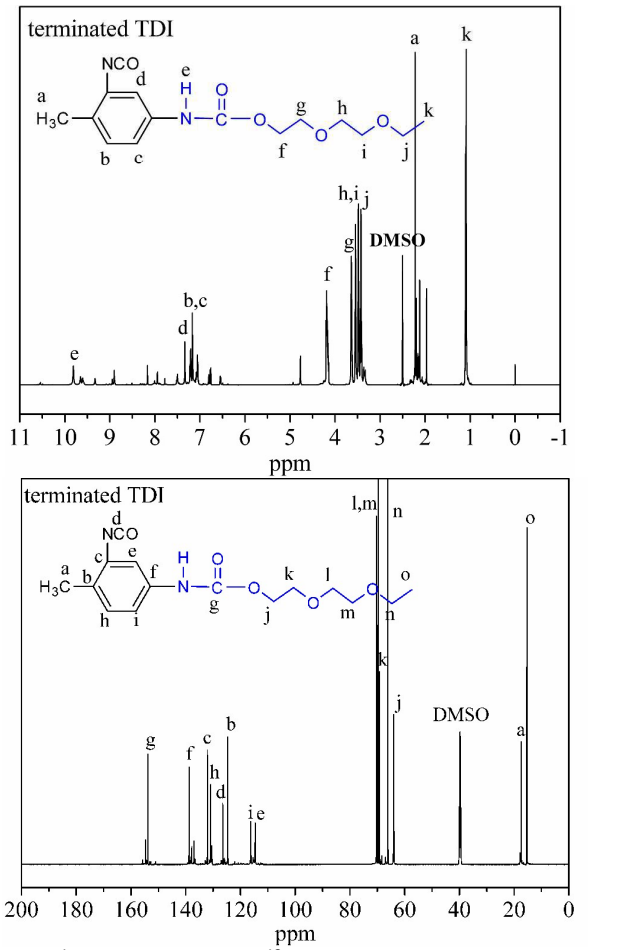

Fig. 2 ^{1}H NMR spectra and ^{13}C NMR spectra of terminated TDI.

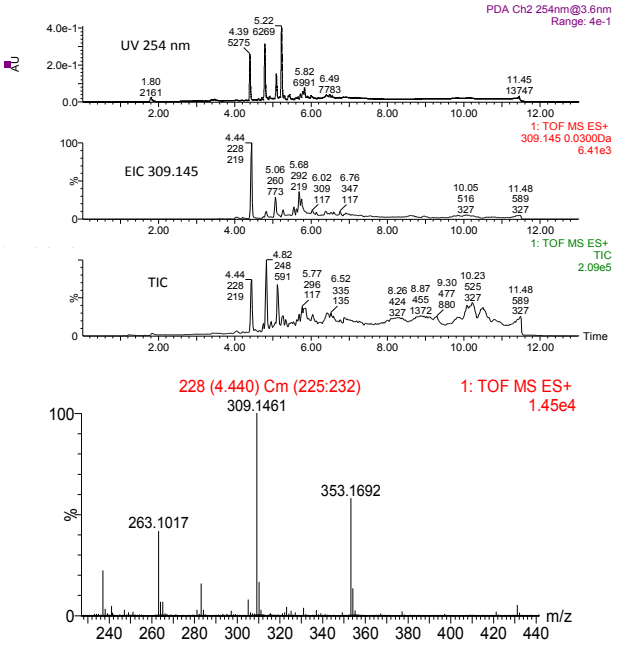

Fig 3. UPLC/Q-TOF-MS and analysis of terminated TDI.

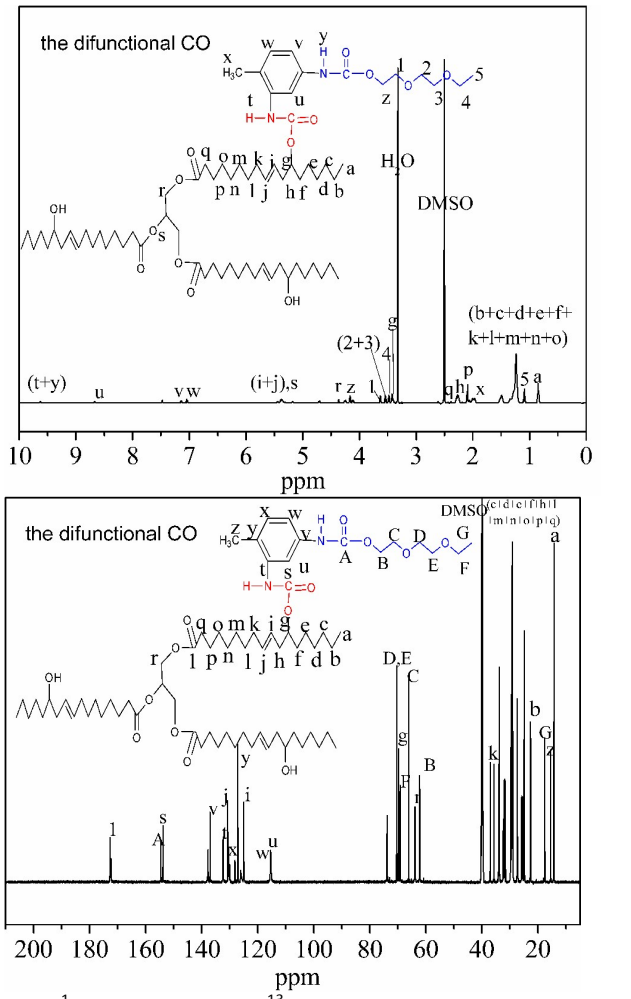

Fig. 4 ^{1}H NMR spectra and ^{13}C NMR spectra of difunctional CO.

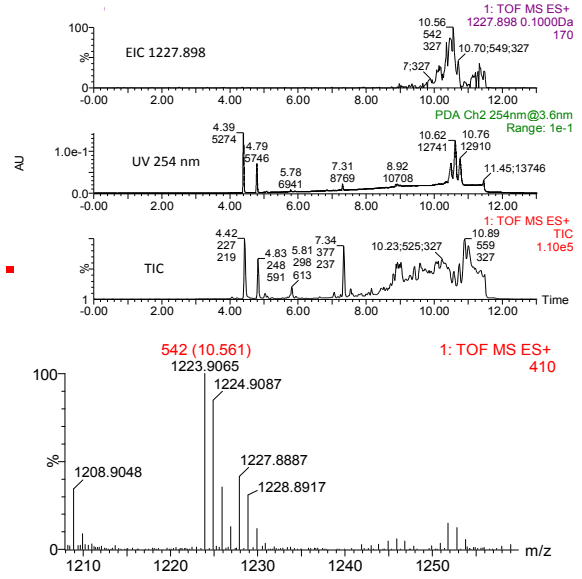

Fig 5. UPLC/Q-TOF-MS and analysis of difunctional CO.

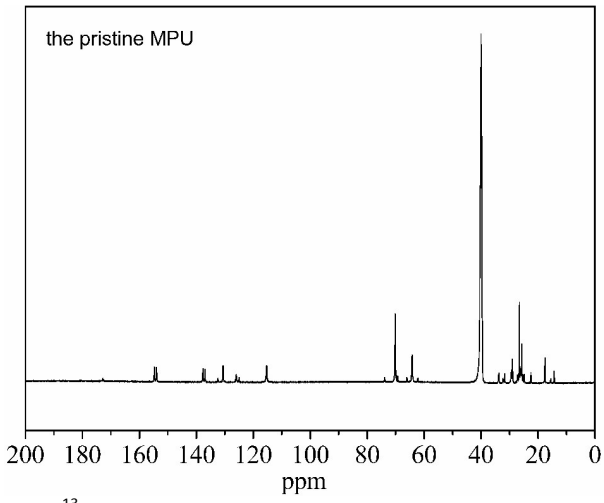

Fig. 6 ^{13}C NMR spectra of D.

NMR spectrometry conform the structures of the synthetic terminated TDI, difunctional CO and D. The ^{1}H NMR spectra and ^{13}C NMR spectra of terminated TDI, as shown in Fig. 2, ^{1}H NMR spectra and ^{13}C NMR spectra of difunctional CO, as shown in Fig. 4 and the corresponding chemical shift values already discussed in Experimental section. The ^{13}C NMR spectrum (Fig. 6) of MPU is divided into two parts. The first part describes the spectrum of the difunctional CO in polymer backbone chain. Peaks around δ 15.5 to 20.8 ppm and δ 28.1 to 28.5 ppm represent the carbon atoms of long chain fatty acid in triglyceride (the difunctional CO). The second part explains the branched structure of MPU present on the the difunctional CO backbone. The signals between δ 113.2 and δ 134.9 ppm are ascribed to the proton in the aromatic ring. The signal at δ 153.8 ppm is ascribed to the proton in the carbamate.

The mass spectra of terminated TDI was shown in the Fig. 3. The $[M+H]^{+}$ m/z 309.1461 formed by add of H to the m/z 388.332 were observed in the mass spectrum. The m/z 309.1462 was fragmented to be m/z 263.1017 by loss of –O-CH_2-CH_3. According to the results of the MS, the structure of teriminated TDI was identified. The mass spectra of difunctional CO was shown in the Fig. 5. The peaks of m/z 1226.89-1229.90 represented difunctional CO. The m/z 1223 and 1224 formed by loss of H from the m/z 1227 were observed in the mass spectrum. The m/z 1223 was further fragmented to be m/z 1208 by loss of -CH_3. According to the results of the UPLC/Q-TOF-MS, the structure of difunctional CO was identified.

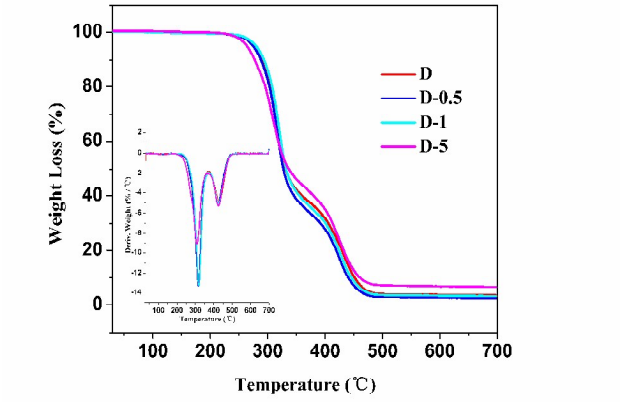

Fig. 7 TGA thermogram of MPU and MPU/HNTs nanocomposites.

Table 2 Thermal properties of pristine MPU and MPU/HNTs nanocomposites, including the onset temperature (T_{onset}) and the temperatures of 10% ($T_{10\,\%}$) and 50% ($T_{50\,\%}$) weight loss.

Samples	T_{onset} (°C)	$T_{10\,\%}$ (°C)	$T_{50\,\%}$ (°C)
D	277	291	331
D-0.5	273	288	327
D-1	279	293	332
D-5	262	276	335

Thermal stability of the composites is an important indicator to its performance, which also reflects the interaction between the components to some extent. Thermal stability of elastomers was studied by TGA analysis. The TGA and DTG curves of the neat MPU and MPU/HNTs nanocomposites containing different HNTs loadings in nitrogen were shown in Fig. 7. As was observed, the thermal decomposition of nanocomposites according to the temperature from low to high were divided into three stages.[44] The first stage starting on the C-O bond of the urethane groups on the main chain of polyurethane nanocomposites were observed, which decomposed into diisocyanate and polyol. At higher temperature, the diisocyanate further decomposed into amines, alkenes and CO_2 corresponding to the second stage of thermal decomposition. In the thermal decomposition process certain portion of the isocyanate products further formed imide, which decomposed into isocyanate at high temperature corresponding to the third stage. As can be seen in the derivative thermogravimetry (DTG) curves, the decomposition processes of the neat MPU and MPU/HNTs nanocomposites were divided into two stages corresponding to the degradation of soft and hard segment domains, in which the first one at about 318 °C was attributed to the dissociation of weaker allophanate, urethane and aliphatic groups. The second peak at about 420 °C related to the aromatic and esteric groups in the polymer backbone. The main results containing the onset temperature (T_{onset}) and the temperatures of 10% ($T_{10\,\%}$) and 50% ($T_{50\,\%}$) weight loss are presented in Table 2.

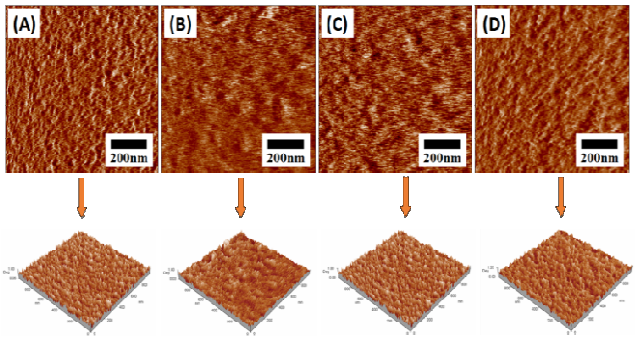

Fig. 8 Surface phase (up), and zoom-in 3D phase (down) diagrams of MPU/HNTs nanocomposites obtained by AFM. (A) D, (B) D-0.5, (C) D-1, and (D) D-5.

Fig. 8 demonstrated AFM diagrams for the surface of pristine MPU and MPU/HNTs nanocomposites. The phase diagrams that reflected the sensitive phase shift between the soft MPU and hard HNTs as well as that between the soft and hard segments of MPU matrix could provide additional information for the surface characteristics of MPU/HNTs nanocomposites. The brightest areas in phase diagrams represented HNTs, while the hard segment of MPU was brighter than the soft segment. As evident from the phase diagrams, when the concentration of HNTs was equal or higher than 1%, a part of HNTs were exposed on the surface. The area of HNTs neighborhood on the surface of the nanocomposites was further analyzed by 3D phase diagrams. On the surface of MPU, the soft segments, which was in the "trough" of the concave portion because of its soft molecular chain and easy motion forming the continuous phase distribution corresponding to the darker portion, were surrounded by the hard segment, which was in the "crest" of the convex portion because of the higher surface energy forming the dispersed phase distribution corresponding to the lighter portion. As HNTs were added into MPU, the region of hard segment turned brighter. These results indicated that the HNTs preferentially reinforced the hard microdomains rather than the soft segments of MPU.

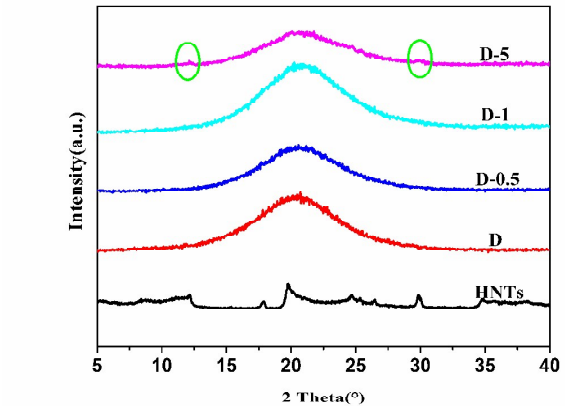

Fig. 9 XRD pattern of HNTs, MPU, and MPU/HNTs nanocomposites.

The X-ray diffraction (XRD) spectra of HNTs, pure MPU, and the MPU/HNTsnanocomposites were presented in Fig. 9. The 2θ angle at 20.09° corresponded to the amorphous diffraction peak of pure MPU,which showed relatively blunt shape, and indicated low degree of crystallinity of the sample. The 2θ angle at 12° and 30°corresponded to the HNTs. The obvious diffraction peak of HNTs was visible owing to the crystalline structure of typical silicate materials. Because of the low content of HNTs, no obvious peaks of halloysite were visible in D-0.5 and D-1, while the peaks centered at 12° and 30° were identified in D-5 sample. In addition, changes of the peak shape with broadening width and increasing intensity around 2θ angle at 20° were visible in D-0.5 and D-1, which was due to the reaction of the OH group of HNTs with the NCO group of MPU. These indicated that the original nanotube structures of halloysite were well preserved in the nanocomposites.

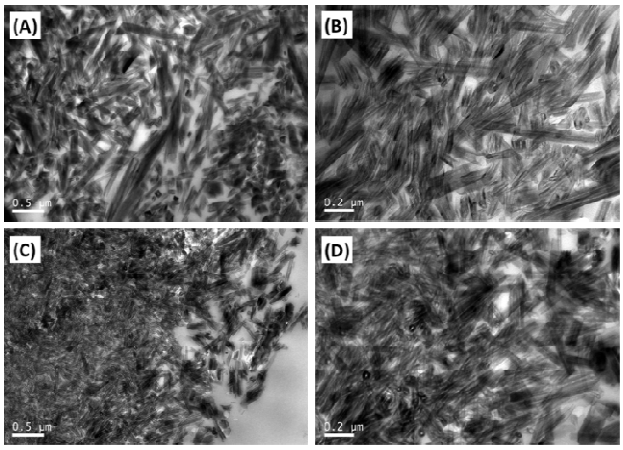

Fig. 10 Transmission electron micrographs of the ultrathin cryo cross-section of MPU/HNTs nanocomposites with 0.5wt% HNTs (A, B) and 5wt% HNTs (C, D).

No large aggregatesof the HNTs in the nanocomposites containing only 0.5 wt% HNTs were observed in Fig. 8 (A, B) by the transmission electron microscopy (TEM), implying good adhesion between fillers and matrix. Such an even and uniform distribution of the fillers in the matrix could play an important role in improving the mechanical performance of the resulting nanocomposite films as discussed later. As was shown in Fig. 10 (C, D), little aggregates of the HNTs were appeared in certain separated domains as shown in the TEM images of the ultrathin cryo cross section of the MPU/HNTs nanocomposite film containing 5 wt % of HNTs.

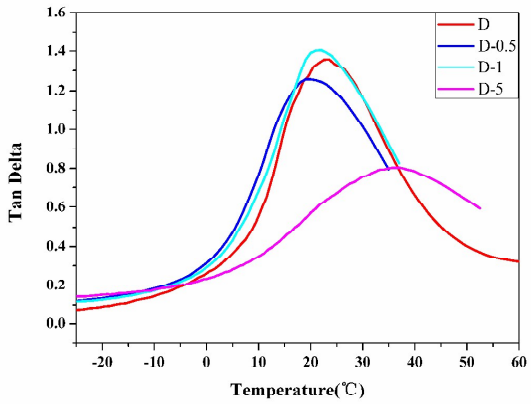

Fig. 11 Damping factor tan δ of MPU and MPU/HNTs nanocomposites as a function of temperature.

The phase separation of MPU resulting from thermodynamic incompatibility between the soft and hard segments played a key role in the physical properties. The glass transition temperature (T_g) of soft segment molecular chains would shift to higher temperature when the compatibility between soft segment and hard segment increased and the micro-phase separation degree decreased. Thus, the phase separation degree of materials can be determined according to the movement about T_g. Damping factor tan δ of the samples as a function of temperature were expressed in Fig. 11. The influence of HNTs on the phase separation structure was also featured by the increase of T_g of the nanocomposites. The increase of T_g for the nanocomposites was due to the fact that the HNTs were intensely associated with the hard segment of MPU. The height and sharpness of the damping peaks indicated the degree of order and the freedom of motion of the molecules in the soft domains. The amplitude of the damping peak corresponding to the glass transition of the products increased with incorporating HNTs, which could be attributed to thegreatly restricted motion of MPU chains resulting from the covalent bondbetween theNCO groups of TDI and theOH group of HNTs. The flexible of soft segment polyurethane matrix shifted to weaker. The result was consistent with the result of FTIR, Raman, AFM and XRD analysis.

Table 3 Physical and mechanical properties of pristine MPU and MPU/HNTs nanocomposites

Samples	Tensile strength (MPa)	Elongation at break (%)	Young's Modulus (MPa)	Hardness (Shore A)
D	20.0	372	213.4	91
D-0.5	26.9	313	348.3	105
D-1	24.1	263	282.7	99
D-5	1.1	442	3.4	65

The introduction of HNTs as the reinforcing filler in MPU led to improvement of tensile strength, elongation at breakof the nanocomposites as summarized in Table 3. The tensile strength was increased from 20.0 MPa of pure MPU to 26.9 MPa of D-0.5 containing only 0.5 wt % HNTs. Analogously, the Young'sModulus was increased from 213.4MPa to 348.3MPa for D-0.5. The sharp decline in the tensile strength of the MPU/HNTs nanocomposites after adding 5 wt% HNTs was observed, which was due to the agglomeration occuring in the polyurethane matrix and thus to affect its mechanical performance. The resultswere consistent with the result of FTIR, Raman, AFM, XRDand TEM analysis.

Conclusions

In this study, NCO-terminated castor oil-based polyurethane with low content of HNTs were synthesized successfully. CO, a bio-based resource polyol, appeared to be a promising alternative to petroleum-based polyols in the manufacture of polyurethane prepolymers. The results obtained from AFM and TEM indicated that the HNTs fillers were well dispersed within the MPU matrix and had good adhesion in the interfacial area owing to the reaction between OH groups of HNTs and NCO groups of TDI. A well dispersion state of the HNTs was crucial to improve the mechanical properties. The individualized HNTs were covalently bonded with the hardmicrodomains of segmented polyether polyurethane, which affected the phase separation of the nanocomposites, and such nanostructure was also crucial to stiffen and toughen the MPU without reducing its extensibility, as characterized by FTIR and DMA. The thermal properties changed slightly as a result of the low content of HNTs. For the mechanicalproperties, the introduce of HNTs improved the tensile strength and hardness of MPU nanocomposites. Among all the samples, the D-0.5 which containing only 0.5wt% HNTs is a better one,its tensile strength and Young's modulus were increased from20.0 MPaand 213.4MPa to 26.9 MPa and 348.3MPa compared to pure MPU, respectively.

Acknowledgments

The authors thank Ningbo Institute of Industrial Technology and Instrumental Analysis Center of SJTU for providing equipments to help with AFM and TEM measurements, respectively.

References

1 S. S. Ray and O. Masami, *Prog. Polym. Sci.*, 2003, **28**, 1539-1641.
2 P. Podsiadlo, A. K.Kaushik, E. M.Arruda, A. M.Waas, B. S.Shim, J. D.Xu, H.Nandivada, B. G.Pumplin, J.Lahann, A.Ramamoorthy and N. A.Kotov, *Science*, 2007, **318**, 80-83.
3 S. M.Liff, N.Kumar and G. H.McKinley, *Nat.Mater.*, 2007, **6**, 76-83.
4 S.S.Narine, X.Kong, L.Bouzidi and P. Sporns, *J. Am. Oil. Chem. Soc.*, 2007, **84**, 55-63.
5 S. A.Madbouly, Y. Xia and M. R.Kessler, *Macromolecules*, 2013, **46**, 4606-4616.
6 Y. Xia and R. C.Larock, Macromol.*RapidCommun*., 2011, **32**. 1331-1337.
7 S. Oprea, *J.Mater*. *Sci*., 2011, **46**, 2251-2258.
8 Y. Hamid and R. M.Mohammad, *Eur*. *Polym*. *J*., 2004, **40**, 1233-1238.
9 L.Jiang, C.Zhang, M. K. Liu,Z.Yang, W. W.Tjiu and T. X. Liu,*Compos*. *Sci*. *Technol*., 2014, **91**, 98-103.
10 W. O.Yah, A.Takahara and Y. M.Lvov, *J. Am. Chem. Soc*., 2012, **134**, 1853-1859.
11 M.Liu,Y.Zhang,C.Wu, S.Xiong and C.Zhou,*Int*. *J. Biol*. *Macromol*.,2012, **51**, 566-575.
12 V.Vergaro, Y. M.Lvov and S.Leporatti, *Macromol*. *Bio*.*Sci*., 2012, **12**, 1265-1271.
13 D.Tao, Y.Higaki,W.Ma,H.Wu, T.Shinohara, T.Yano and A.Takahara,*Polymer*,2015, **60**, 284-291.
14 M.Liu,Z.Jia,D.Jia and C.Zhou,*Prog*. *Polym*.*Sci*., 2014, **39**, 1498-1525.
15 B.Lecouvet,M.Sclavons, S.Bourbigot,J.Devaux and C.Bailly, *Polymer*, 2011,**52**, 4284-4295.
16 J. K.Mishra,I.Kim and C. S.Ha, Macromol. *Rapid*.*Commun*., 2003, **24**, 671-675.
17 J. K.Mishra,I.Kim and C. S.Ha, Macromol.*Rapid*. *Commun*., 2004, **25**, 1851-1855.
18 N. G.Shimpi,H. A.Sonawane,A. D.Mali and S.Mishra, *Polym*. *Bull*., 2014,**71**, 515-531.
19 A. K.Barick and Y. W.Chang,*High*. *Perform*. *Polym*., 2014, **26**, 609-617.
20 J. Ahenmiller and D. Patterson, *RubberWorld*, 1993, **27**.
21 S.Turri, R.Valsecchi,M.Levi,M.Cristin and A.Sanguineti,*Eur*. *Polym. J.*, 2008, **44**, 2951-2961.
22 N. D.Ghatge and V. B.Phadke, Rub*b*er *Age*, 1968,**10**,52.
23 T. L.Jablonowski and R. J.Scribner,151st ACS Rubber Division Meeting, Spring, Anaheim Ca.,1997, Paper 61, p. 19. 012.
24 J. R. Serumgard. 151st ACS Rubber Division Meeting, Spring, Anaheim Ca., 1997, Paper 12, p. 19. 012.
25 J.Ahnemiller,*Rubb*.*PlastNews*., 1992, **21**, 15.
26 P. H. McKinstry and M.Chase,Urethanes Technology(1990), April - May,24-28.
27 S. K. N.Kutty and G. B.Nando,Plast.*Rubber Process. Appl.*, 1990, **14**, 109-117.
28 H. Shirasaka, US Pat., 6008312, 1999.
29 A. Singh, US Pat., 4335231, 1982.
30 S. Turri, M. Levi, M. Cristini and A. Sanguineti, *Polym*. *Int*., 2005, **54**, 698-704.
31 D.Cai, K.Yusoh and M.Song,*Nanotechnology*, 2009, **20**, 685-712.
32 B. X. Fu, B. S.Hsiao, H.White,M.Rafailovich,P. T.Mather,H. G.Jeon,S.Phillips,J.Lichtenhan and J.Schwab,*Polym*. *Int*., 2000, **49**, 437-440.
33 H. Liu, J.Xu, Y.Li, B.Li, J.Ma and X.Zhang, Macromol. *RapidCommun*., 2006,**27**, 1603-1607.
34 R.Sen, B.Zhao, D.Perea,M. E.Itkis,H.Hu,J.Love,E.Bekyarova and R. C.Haddon, *Nano*.*Lett*., 2004, **4**, 459-464.
35 H.Koerner,W. D.Liu, M.Alexander, P.Mirau, H. Dowty and R. A.Vaia,*Polymer*, 2005, **46**, 4405-4420.
36 H. S.Xia and M.Song, *SoftMatter*, 2005,1, 386-394.

37 J.Kwon and H. Kim,*J. Polym. Sci. Part A: Polym. Chem*., 2005, **43**, 3973-3985.
38 S. M.Liff, N.Kumar and G. H.McKinley, *Nat*. *Mater*., 2007, **6**, 76-83.
39 Z.Wang and T. J.Pinnavaia, *Chem*. *Mater*., 1998, **10**, 3769-3771.
40 C.Zilg, R.Thomann, R.Mülhaupt and J.Finter, *Adv*. *Mater*., 1999, **11**, 49-52.
41 Y. I.Tien and K. H.Wei, *Macromolecules*, 2001, **34**, 9045-9052.
42 B.Finnigan, K.Jack, K.Campbell, P.Halley, R. Truss, P.Casey, D.Cookson, S.King and D.Martin,*Macromolecules*, 2005, **38**, 7386-7396.
43 R. L. Frost and H. F. *Shurvell*, *Clay*. *Clay*. *Miner*., 1997, **45**, 68-72.
44 N. Yoshitake and M. Furukawa, *J. Anal. Appl. Pyrolysis.*, 1995, **33**, 269-281.

the Table of Contents

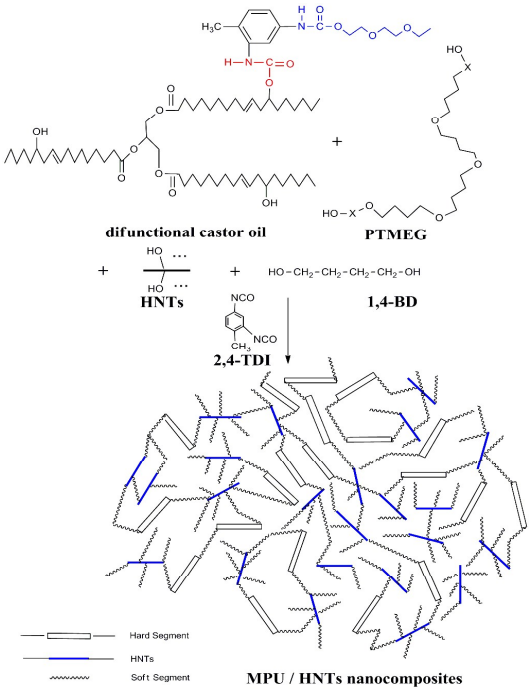

Reaction scheme for the synthesis of elastomeric gum polyurethanes nanocomposites.